COMMUNICATION

Universal Formation of Compositionally Graded Bulk Heterojunction for Efficiency Enhancement in Organic Photovoltaics

Zhengguo Xiao, Yongbo Yuan, Bin Yang, Jeremy VanDerslice, Jihua Chen, Ondrej Dyck, Gerd Duscher, and Jinsong Huang*

The discovery of bulk heterojunction (BHJ) structures paved the road for high efficiency energy conversion by organic photovoltaic devices (OPVs) in the last decade.[1–9] The morphology of BHJ films plays a critical role in charge generation, collection, or recombination in BHJ OPV devices.[10–16] An ideal BHJ film morphology was suggested to have a bicontinuous interdigitated donor and acceptor network with donor and acceptor nanodomains within the exciton diffusion lengths or the uncertain length of light[17,18] for efficient charge generation and extraction.[10–12,14,19] However, the actual morphologies of most BHJ films are generally far from ideal due to the random mixing of donor and acceptor in solution. Regular BHJ films fabricated from the blended solution inevitably have many breaks and dead ends.[1,12] Strategies such as thermal annealing,[13,20–22] solvent annealing,[23] and mixing additives[3,24,25] have been shown to successfully improve the morphologies of some BHJ films by increasing crystallinity of the donors and acceptors and/or forming nanodomains of donors and acceptors with suitable domain size to facilitate exciton dissociation and charge generation. However, these methods did not address the connectivity of the donor and acceptor network and are only applicable to specific material systems. On the other hand, attempts to form the ideal BHJ structures using pre-formed n-type nanorod/ nanowire arrays followed by infiltration of semiconducting polymers have not resulted in PCEs comparable to those made of blended films, which might be limited by interface issues.[26] Another issue with regular BHJ films is the mismatch between the photocurrent distribution and charge transport channel width in the vertical direction: electron current is higher toward the cathode side, and hole current is higher toward anode side due to nonsymmetrical charge collection in OPVs,[27,28] while the distribution of donors and acceptors in regular BHJ films is generally uniform due to the uniform mixing of them in solution. This mismatch could cause the photogenerated charges piling up which end up with recombination. It can severely reduce device PCE when the photogenerated charge density is high, in cases such as low bandgap active layers and under strong illumination, or when photogenerated charges cannot be efficiently extracted out of the active layer due to low carrier mobility or a thick active layer.[29,30] All of these nonideal morphologies inevitably cause the charge recombination both in the BHJ films and at the metal/organic interface, in forms of geminate recombination,[31,32] or bimolecular recombination.[33,34]

Compositionally graded BHJ films, donor enriched at the anode and acceptor enriched at the cathode side, were proposed to facilitate the charge extraction and to reduce charge recombination in several highly efficient OPVs, such as poly(3-hexylthiophene) (P3HT): C_{61}-butyric acid methyl ester ([60]PCBM) and poly[(4,4′-bis(2-ethylhexyl)dithieno[3,2-b;2′,3′-d]silole)-2,6-diyl-alt-(4,7-bis(2-thienyl)-2,1,3-benzothiadiazole)-5,5′-diyl] (PSBTBT): [60]PCBM.[20,22,35–37] The higher donor content at the top surface also explains the higher PCEs in their inverted structure device than in the regular structure device. As illustrated in **Figure 1**, the composition profile of the graded BHJ films with a donor rich anode side and an acceptor rich cathode side better matches the distribution of current, which should reduce the piling up of electrons close to the cathode side and holes close to the anode side and reduce the leakage of photogenerated charges to the wrong electrodes, thus reducing bimolecular charge recombination.[37–39] However, the graded BHJs with preferred composition profiles were only observed in a few high efficiency material systems which require special substrate surfaces and suitable surface energy differences between donors and acceptors for its formation.[20,35] In addition, these graded BHJs do not necessarily provide better bicontinuous connectivity of donors and acceptors. Here, we report a method to effectively form the graded BHJ by a very simple solvent-fluxing process which is applicable to all solution-processed BHJ films which involves additives. The fluxing process also improved the morphologies of the BHJ films by forming more uniform [70]PCBM domain distribution in the plane direction of the films and resulted in higher charge collection efficiency. As a result, PCE enhancements by 15–50% are achieved for all graded BHJ systems tested compared with the optimized regular BHJ OPVs.

Z. Xiao, Y. Yuan, B. Yang, J. VanDerslice, J. Huang
Department of Mechanical and Materials Engineering
and Nebraska Center for Materials and Nanoscience
University of Nebraska-Lincoln
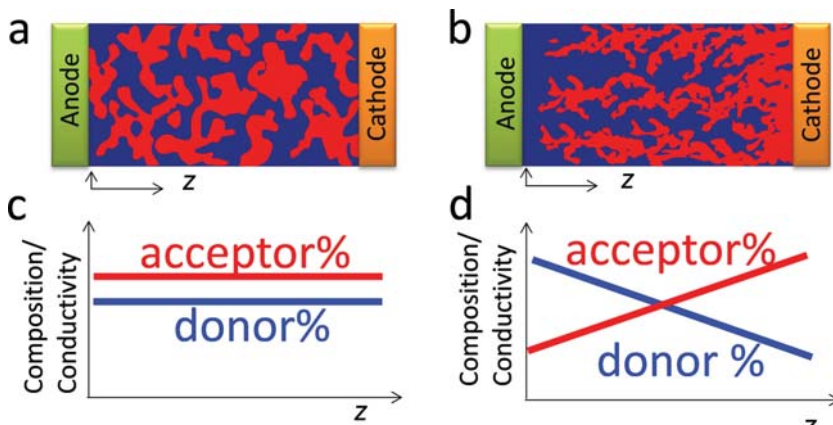Lincoln, NE 68588–0526
E-mail: jhuang2@unl.edu
J. VanDerslice
J.A.Wollam Co., Inc
Lincoln, NE 68508
J. Chen
Center for Nanophase Materials Sciences
Oak Ridge National Laboratory
Oak Ridge, TN 37831–6494
O. Dyck, G. Duscher
Department of Materials Science and Engineering
University of Tennessee
Knoxville, TN 37996–2100

Figure 1. (a–b) Illustration of the morphology of donor (blue) and acceptor (red) distribution in regular and graded BHJ devices. Composition profile of donor and acceptor in regular (c) and graded (d) BHJ devices. A larger composition percentage is correlated with wider charge transportation path and thus larger effective conductivity.

The schematics of the method using solvent-fluxing to form graded BHJ are shown in **Figure 2**. Firstly, a high boiling point

additive 1,8-diiodooctane (DIO) was added to the polymer donors: fullerene-derivative solutions. After spin coating the blended solution on top of indium tin oxide (ITO)/poly(3,4-ethylenedioxythiophene):poly(styrenesulfonate) (PEDOT:PSS) substrate, the working solvent, such as 1,2-Dichlorobenzene (DCB), evaporated while DIO stayed in the blend film for a long time due to its high boiling temperature of 333 °C. It was found that the blended films were still wet and sticky after one day of storage at room temperature, indicating the extremely slow evaporation of DIO. Previous study shows that DIO is a better solvent for fullerene-derivatives (>120 mg/mL for PCBM) than traditional solvents, such as chlorobenzene, because of their strong interactions caused by the partial negative charge of iodine in DIO and electro-deficient property of fullerene-derivatives.[40] DIO then grasped fullerene-derivatives into nanodroplets during evaporation of DCB.[40,41]
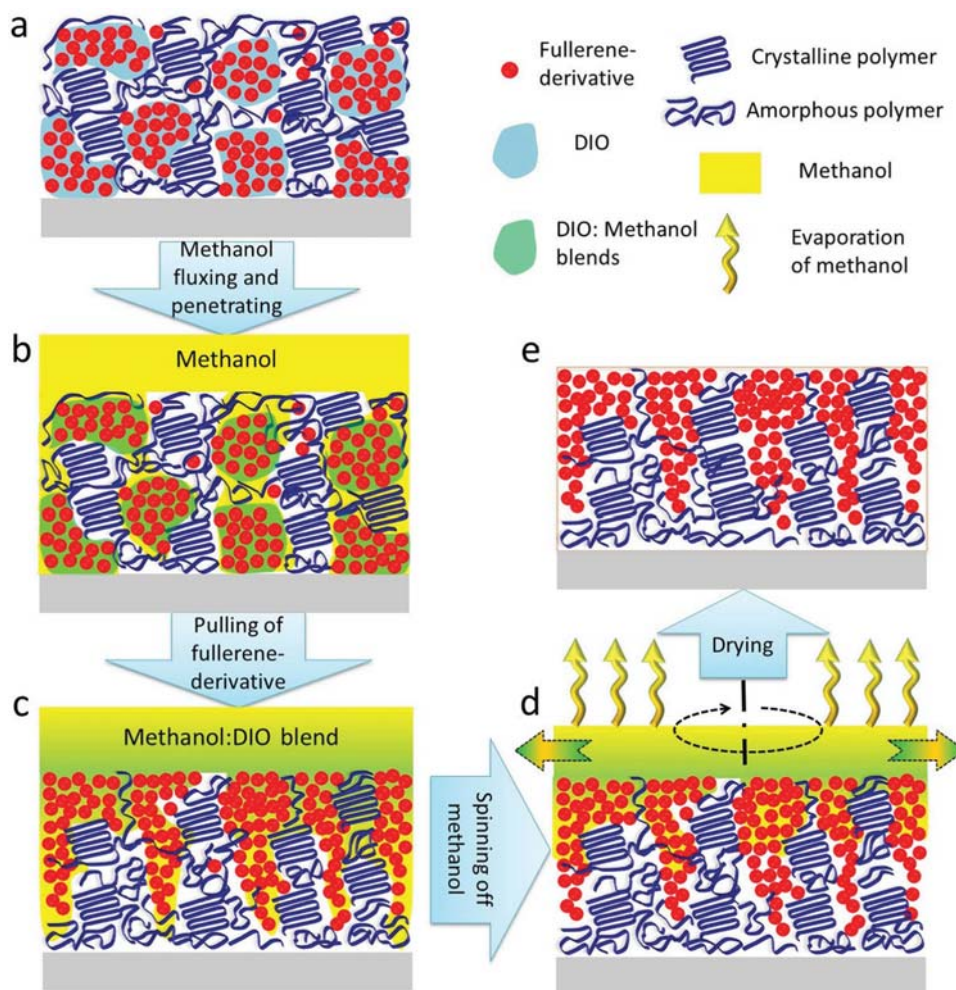

Figure 2. (a), Formation of DIO:fullerene-derivatives nano-droplets after the spin coating of the polymer:fullerene-derivatives blend solution with DIO as additive; (b), Penetration of methanol into the blend film along the DIO regions; (c), Extraction of DIO as well as partial fullerene-derivatives to the surface; (d), Removing DIO with methanol from the film by spin coating; (e), Formed graded BHJ with better connectivity of donors and acceptors.

© 2014 WILEY-VCH Verlag GmbH & Co. KGaA, Weinheim

Secondly, the wet blended films were fluxed with low boiling point solvents, such as methanol (Figure 2b). Methanol does not dissolve fullerene-derivatives or semiconducting polymers but mixes very well with DIO. Therefore, after dripping methanol on the top of the blended films, methanol quickly penetrated into the wet films, dissolved the DIO, and connected the DIO:fullerene-derivative nanodroplets, as illustrated in Figure 2b. DIO dissolved in methanol diffused to the surface of the films, indicated by the quick darkening of the film after dripping methanol onto the film because solid-state fullerene has much stronger absorption in visible range than fullerene solution. The fast extraction of DIO from inside of the BHJ film brings some fullerene-derivatives dissolved in DIO toward the film surface and thus forms the graded composition in the vertical direction, as illustrated in Figure 2c. Thirdly, while methanol was spun off of the surface of the film, DIO was fluxed away by methanol (Figure 2d), leaving the deeper colored graded BHJ films after methanol dried (Figure 2e). The graded BHJ structure, with an increasing fullerene-derivative percentage from bottom to top, formed after methanol dried. The donor polymers used included P3HT, poly[4,8-bis-(2-ethyl-hexyl-thio-phene-5-yl)-benzo[1,2-b:4,5-b']dithiophene-2,6-diyl]-alt-[2-(2'-ethyl-hexanoyl)-thieno[3,4-b]thiophen-4,6-diyl] (PBDTTT-CT), poly[N-9'-hepta-decanyl-2,7-carbazole-alt-5,5-(4',7'-di-2-thienyl-2',1',3'-enzothiadiazole)] (PCDTBT), and Poly[6-fluoro-2,3-bis-(3-octyloxyphenyl) quinoxaline-5,8-diyl-alt-thiophene-2,5-diyl] (FTQ) and the acceptor materials included Phenyl-C_{71}-Butyric-Acid-Methyl Ester ([70]PCBM) and indene-C_{60} bisadduct ([60]ICBA). The chemical structures of the donors and acceptors are shown in Figure S1. Two high efficiency material systems, PBDTTT-CT:[70]PCBM and PCDTBT:[70]PCBM, were focused on in the following material and device characterizations.

The extraction of DIO by methanol-fluxing can be observed by the naked eyes because of the color change of the BHJ films. The dried BHJ films have deeper color than the wet film due to the stronger Pi-Pi conjugation between the solid semiconductor molecules, which were observed in all of the BHJ films tested. **Figure 3** shows pictures of PBDTTT-CT:[70]PCBM and PCDTBT:[70]PCBM films with partial areas fluxed and the corresponding absorption spectra measured at both fluxed and pristine areas. The methanol-fluxed areas are darker than the rest for both PBDTTT-CT:[70]PCBM and PCDTBT:[70]PCBM films. The absorption spectra in the fluxed areas are almost identical to those of the overnight, vacuum-dried BHJ films. This gives a direct correlation between the color changes and the extraction of DIO by solvent-fluxing. The difference between methanol-fluxing and vacuum-drying of DIO is that the quick extraction of DIO nanodroplets by methanol will also pull some fullerene-derivatives toward the BHJ film surfaces and thus form the graded BHJs.

The formation of graded BHJs by methanol-fluxing was verified by multiple characterization methods. First, the formation of the graded BHJs was revealed by measuring the vertical composition profile of PBDTTT-CT:[70]PCBM and PCDTBT:[70]PCBM films using Energy-Filtered Transmission Electron Microscopy (EFTEM). The low energy plasmon peak (19 ± 4eV) of polymer donors[42–44] was used to highlight the donor so that brighter regions (higher gray value) represent donor-rich region in the EFTEM images. The following conclusions can be drawn from the FETEM images (**Figure** 4a–d) as well as the gray value distribution of the vacuum-dried and fluxed films (Figure 4e-f): 1) The PBDTTT-CT content along the vertical direction in the vacuum-dried PBDTTT-CT:[70]PCBM film is almost constant, while there is a spontaneous un-favored composition gradient in the vacuum-dried PCDTBT:[70]PCBM with PCDTBT rich at the top surface (cathode side). 2) There is a clear graded distribution of the PBDTTT-CT and [70]PCBM in the fluxed film with linearly increasing PBDTTT-CT content toward the PEDOT:PSS (anode side), as shown by the gray value in Figure 4f; The composition gradient of the PCDTBT:[70]PCBM film was completely reversed after solvent-fluxing, leaving a PCDTBT-rich region close to the PEDOT:PSS which is favored for higher efficiency in the regular structure device. 3) The distribution of polymers and [70]PCBM in the vacuum-dried PBDTTT-CT:[70]PCBM and PCDTBT:[70]PCBM films is nonuniform in the film plane. There are some randomly distributed, large [70]PCBM-rich regions with size ranging from 50–200 nm. Both fluxed BHJ films have more uniform polymer and [70] PCBM domain distribution in the film plane.

Second, spectroscopic ellipsometry measurements were performed to quantitatively verify the vertical composition
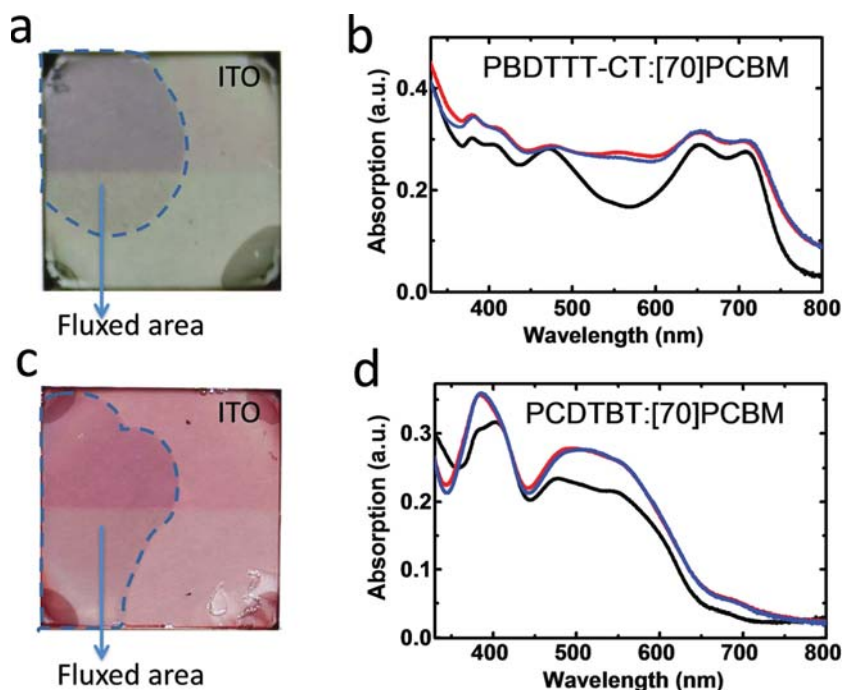
Figure 3. Optical images of PBDTTT-CT:[70]PCBM (a), PCDTBT:[70]PCBM(c),b,d single path absorption spectroscopy of as-prepared (black line)and methanol-fluxed (red line) and vacuum-dried (blue line) films of PBDTTT-CT:[70]PCBM (b), PCDTBT:[70]PCBM(d).
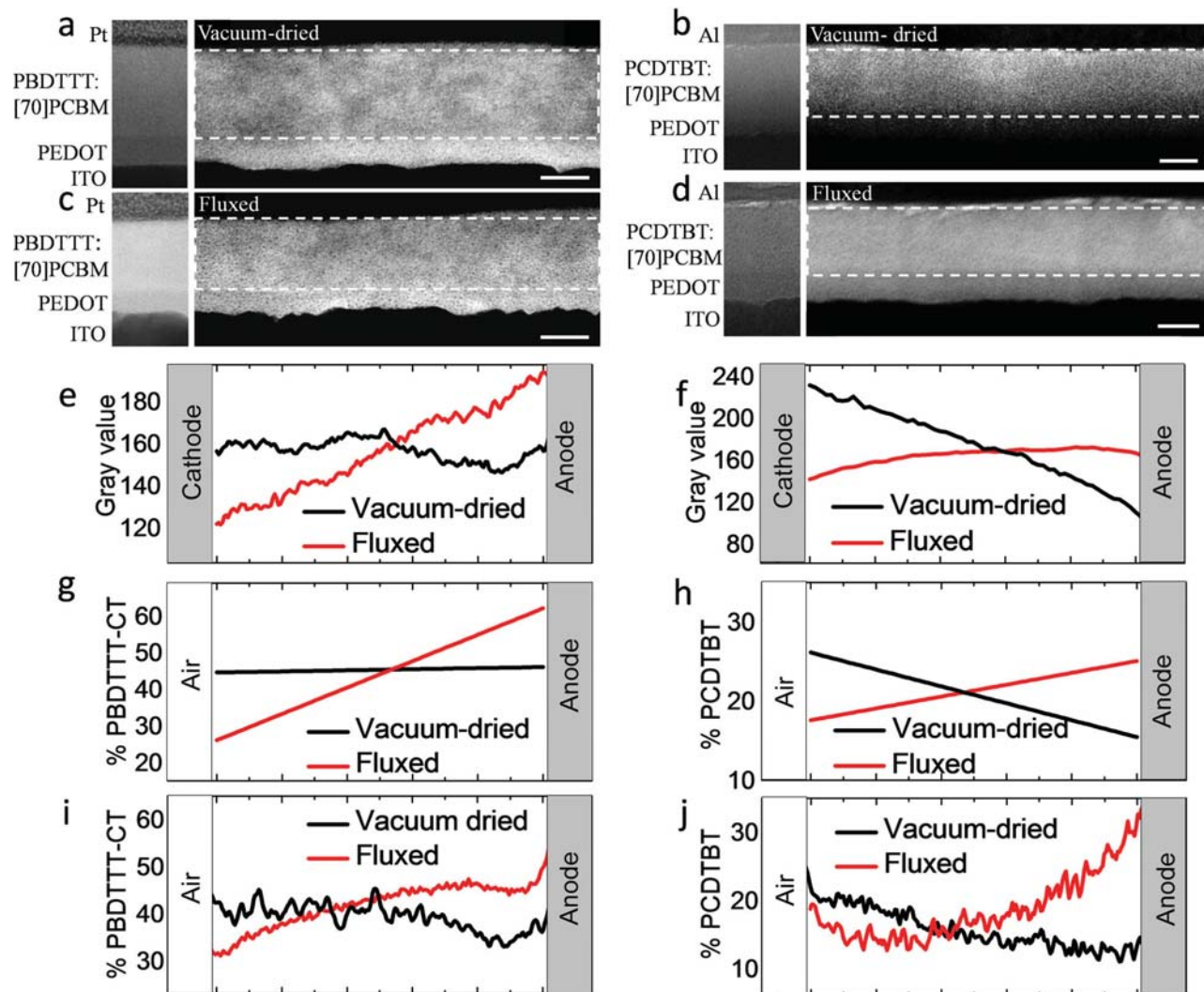
Figure 4. a–d, EFTEM cross-sectional images of the vacuum-dried (a), fluxed PBDTTT-CT:[70]PCBM film (c), vacuum-dried (b), and fluxed PCDTBT:[70] PCBM film (d) with energy filter set at 19 ± 4 eV where brighter regions represent donor-rich region. The small pictures on the left of each EFTEM image are TEM images with energy filter set at 0 V which show each layer clearly, in which donors and acceptors do not have any significant contrast because they have very little differences in terms of their electron density; e,f, Gray values, along the vertical direction, of the vacuum-dried and fluxed PBDTTT-CT:[70]PCBM films (e), and PCDTBT:[70]PCBM films (f) in the areas marked with white dashed squares on the left EFTEM images; (g–h), Quantitative determination of the composition of the vacuum-dried and fluxed PBDTTT-CT:[70]PCBM films (g) and PCDTBT:[70]PCBM films (h) along the vertical direction by ellipsometry; i,j, The composition depth profiles of PBDTTT-CT:[70]PCBM films (i) and PCDTBT:[70]PCBM (j) films measured by SIMS. All the scale bars are 50 nm.

profile.[20] The PBDTTT-CT:[70]PCBM and PCDTBT:[70]PCBM blends were spun on silicon wafers coated with PEDOT:PSS to maintain the same surface condition as the working device while reducing the complexity of the model required to analyze the ellipsometric data. The optical properties of PEDOT:PSS, PBDTTT-CT, PCDTBT, and [70]PCBM were determined individually (Figure S2) and were held fixed when calculating the vertical phase separation. The blended films were discretized into eleven equal segments in the vertical direction, and the percentage of PBDTTT-CT in each segment was allowed to vary in accordance with the Bruggeman effective medium approximation.[45] A linear variation in the PBDTTT-CT and PCDTBT percentage provided the best fit to the experimental data while maintaining a unique solution for the vertical compositional

profile. The ellipsometric measurement utilized a 300 µm diameter beam so the measurement reflects the average condition of the sample and does not resolve the fine spatial variations in the compositional profile. The analysis procedure used to model the ellipsometric data is stated in the supporting materials. As shown in Figure 4g–h, the vacuum-dried PBDTTT-CT:[70] PCBM film has nearly uniform composition distribution in the vertical direction. Whereas, the fluxed PBDTTT-CT:[70]PCBM film has a clear composition gradient with more PBDTTT-CT on the bottom surface. The vacuum-dried film of PCDTBT:[70] PCBM blended film has a spontaneous graded composition with PCDTBT rich at the top surface. After methanol-fluxing, the [70] PCBM was extracted toward the top surface which is favored for the regular BHJ device. Both results agree well

with the EFTEM result. The blended film structure was modeled using a graded effective median approximation where the weight percentage of PBDTTT-CT in PBDTTT-CT: [70]PCBM blended films at the bottom (anode) and top (cathode) interfaces was determined to be 60% and 27%, respectively. The weight percentage of PCDTBT in PCDTBT:[70]PCBM blended films at the bottom and top interfaces was determined to be 25% and 17% respectively, which is in good accordance with the weight ratio of polymer in the blended film (40% for PBDTTT-CT:[70]PCBM and 20% for PCDTBT:[70]PCBM system).

Third, secondary ion mass spectrometry (SIMS) was conducted to directly measure the composition profile of the BHJ films. The content of the polymer was derived from the sulfur atom ratio in the BHJ films, and the results were shown in Figure 4i, j. The weight percentage of PBDTTT-CT of the vacuum-dried film is relatively uniform across the whole film, while it increases linearly with depth in the fluxed film. After methanol-fluxing, the PBDTTT-CT content on the top of the film reduced to 30 wt%, while that at the bottom of the film increased to 51 wt%. The same variation trend of composition profile was observed for vacuum-dried and methanol-fluxed PCDTBT:[70]PCBM films. The composition profile of PCDTBT of the vacuum-dried PCDTBT:[70]PCBM showed a negative slope, while the slope was changed to positive in methanol-fluxed PCDTBT:[70]PCBM film. These results are in excellent agreement with the EFTEM and ellipsometric results and the weight ratio of polymers in the BHJ films, which further

confirms the formation of gradient BHJ films by the solvent-fluxing method.

The photocurrent density-voltage (J_{ph}-V) characteristics of vacuum-dried and solvent-fluxed devices as well as the reflective absorption (RA), external quantum efficiency (EQE) and internal quantum efficiency (IQE) of PBDTTT-CT:[70]PCBM, PCDTBT:[70]PCBM are shown in **Figure 5**. The device's performance of PBDTTT-CT:[70]PCBM, PCDTBT:[70]PCBM, P3HT:[60]ICBA, FTQ:[70]PCBM is summarized in **Table 1** with statistics based on more than 20 devices for each category. The PCEs of PBDTTT-CT:[70]PCBM, PCDTBT:[70]PCBM, P3HT:[60]ICBA, FTQ:[70]PCBM after solvent-fluxing were increased from 6.9% to 8.6%, 5.4% to 7.2%, 4.9% to 6.0%, and 4.4% to 6.0%, respectively. The fabrication parameters and the optimized DIO percentages for each material system are shown in Table SI. The fill factor (*FF*) of 62.5%, IQE of 90% and efficiency of 8.6% for PBDTTT-CT:[70]PCBM based devices, and *FF* of 67.3%, IQE of >90% and efficiency of 7.2% for PCDTBT:[70]PCBM based devices are the highest reported values for these material systems. The slight V_{OC} variation might be caused by the interplay of various effects of solvent fluxing: passivation effect increases V_{OC} while increased crystallinity reduces V_{OC}. The solvent-fluxing method reported here is a new paradigm to optimize the efficiency of some material systems, such as PBDTTT-CT:[70]PCBM and FTQ:[70]PCBM, that cannot be further improved by other established approaches, including thermal annealing, solvent annealing, or additives.
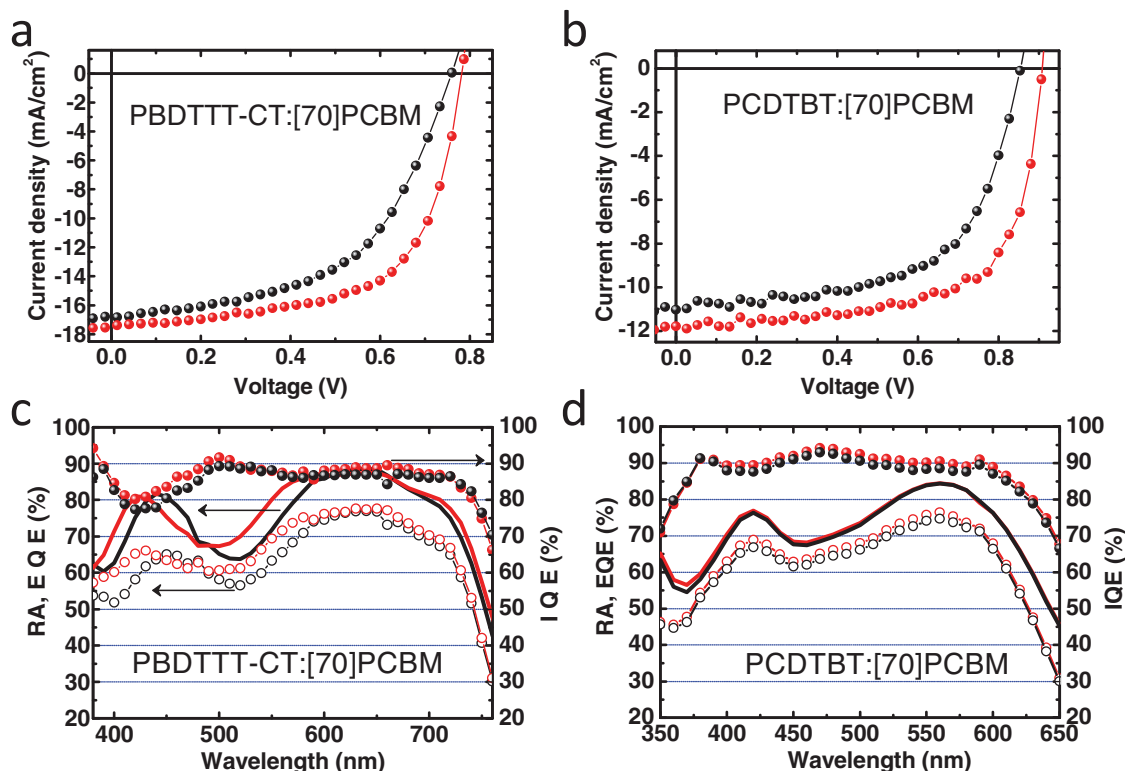
Figure 5. Photocurrent of vacuum-dried (black circle line) and fluxed (red circle line) devices of PBDTTT-CT:[70]PCBM (a), PCDTBT:[70]PCBM (b) under simulated A.M 1.5 illumination. External quantum efficiency (EQE) (open circle lines), reflective absorption (RA) (solid lines) and internal quantum efficiency (IQE) (solid circle lines) of (c) PBDTTT-CT:[70]PCBM and (d) PCDTBT:[70]PCBM devices (black: vacuum-dried, red: fluxed).

Table 1. Statistics of PCE of different kinds of solar cells with regular BHJ (vacuum-dried) and Graded BHJ (solvent-fluxed) structure.

Materials	Blend film drying methods	J_{SC} (mA/cm^2)	V_{OC} (V)	FF (%)	PCE Average	PCE Best
PCDTBT: [70]PCBM	Vacuum-dried	10.5 ± 0.4	0.89 ± 0.01	55.0 ± 0.5	5.20% ± 0.20	5.4%
	Methanol-fluxing	11.5 ± 0.4	0.92 ± 0.01	65.7 ± 0.7	6.95% ± 0.15	7.2%
PBDTTT-CT: [70]PCBM	Vacuum-dried	16.4 ± 0.4	0.76 ± 0.01	53.5 ± 0.5	6.90% ± 0.10	7.0%
	Methanol-fluxing	17.2 ± 0.3	0.78 ± 0.01	63.3 ± 0.7	8.40% ± 0.20	8.6%
P3HT: [60]ICBA	Vacuum-dried	9.8 ± 0.2	0.82 ± 0.01	60.9 ± 0.5	4.90% ± 0.10	5.0%
	Methanol-fluxing	10.3 ± 0.2	0.80 ± 0.01	72.1 ± 0.3	5.90% ± 0.10	6.0%
FTQ: [70]PCBM	Vacuum-dried	9.8 ± 0.3	0.88 ± 0.01	50.0 ± 0.8	4.20% ± 0.20	4.4%
	Methanol-fluxing	10.9 ± 0.2	0.88 ± 0.01	61.3 ± 0.5	5.80% ± 0.20	6.0%

A general guideline is prescribed for the formation of graded BHJ by the solvent-fluxing method: 1) The boiling point of the solution additive must be higher than the working solvent so that only the additive remains in the blended films before the fluxing process; 2) The additive should selectively dissolve fullerene-derivatives so that it brings fullerene-derivatives to the surface during the solvent-fluxing process; 3) The fluxing solvent should mix well with additive but not dissolve polymers or fullerene-derivatives, so that it can pull the additive as well as fullerene-derivatives to the surface and only wash off the additive; and 4) There is an optimal time interval between the deposition of the active layer and the solvent-fluxing so that the fullerene-derivative extraction process does not interrupt or damage the polymer crystallization. Previous studies show that the working solvent drying process plays an important role in determining the morphology of BHJs because the self-organization of polymer predominately occurs in wet films.[23] It is expected that performing the solvent-fluxing process too early interrupts the polymer crystallization, while performing the solvent-fluxing process too late is not effective in extracting fullerene-derivatives because the framework of the polymer will be too rigid. The photocurrent curves of the devices with different time intervals are shown in Figure S6. It was found that a time interval of 10 minutes was optimal for the PBDTTT-CT:[70]PCBM, PCDTBT:[70]PCBM, and FTQ:[70]PCBM-based devices, and 30 min for a P3HT:[60]ICBA-based device. 4) The thickness of the active layer should match the penetration depth of the methanol solvent so that DIO near the PEDOT:PSS side can also be extracted out. From the various characterizations on the PBDTTT-CT:[70]PCBM (100 nm) and PCDTBT:[70]PCBM (80 nm) films shown in Figure 3, the depth composition profile of the films can be modified at the PEDOT:PSS side, which indicates the penetration depth of the methanol is larger than 100 nm.

To test the versatile and universal application of this approach, several other low boiling point solvents, including methanol, ethanol, and isopropanol, were tested for the fluxing process. All of these low boiling point solvents mix well with DIO and do not dissolve fullerene-derivatives or the donor polymers. The device performance using these solvents is shown in Figure S7. All of them resulted in almost the same device performance enhancement compared to the vacuum-dried devices.

It is noted that methanol treatment was used recently to improve the efficiency of thieno[3,4-b]-thiophene/

benzodithiophene (PTB7):[70]PCBM devices, which is ascribed to the passivation of surface traps and a corresponding increase of surface charge density.[46] In that study, the PTB7:[70]PCBM films were first vacuum-dried to remove DIO; therefore, the methanol-fluxing can only cause surface passivation rather than change the morphology or vertical composition distribution inside the BHJ films. To manifest their difference, the performances of the PBDTTT-CT:[70]PCBM and PCDTBT: [70]PCBM devices were compared using these two different solvent treatments, and the photocurrents were shown in **Figure 6**. Efficiency enhancements were observed rising from 6.9% to 7.4% for PBDTTT-CT:[70]PCBM devices and from 5.0% to 6.0% for PCDTBT:[70]PCBM devices after methanol-fluxing of the vacuum-dried films, which can be ascribed to the reported surface passivation effect. In contrast, methanol-fluxing of the wet films gave much higher efficiencies of 8.6% for PBDTTT-CT:[70]PCBM and 7.2% for PCDTBT:[70]PCBM devices, demonstrating the importance of the graded BHJs in efficiency enhancement.

In order to further examine the contribution of the graded structure on the performance enhancement of the solvent-fluxed BHJ devices, inverted structure devices were fabricated with a device structure of: ITO/ Cesium carbonate (Cs$_2$CO$_3$) (0.3 nm)/PBDTTT-CT(or PCDTBT):[70]PCBM (80–100 nm)/ Molybdenum trioxide (MoO$_3$) (8 nm)/Ag. Such inverted structure devices give comparable device performances with regular structure BHJ devices if the BHJ films were vacuum-dried as shown in Figure 6c-d. After a methanol-fluxing process which brings [70]PCBM to the top surface, both J_{SC} and FF reduced in the inverted graded BHJ devices, and the PCE of the devices decreased from 6.8% to 6.2% for PBDTTT-CT:[70]PCBM devices, and from 5.0% to 4.1% for PCDTBT:[70]PCBM devices, respectively. This result excludes the other factors, including enhanced carrier mobility, molecular crystallinity and/or orientation variation (if there is) by the solvent-fluxing process, and confirmed graded BHJ junctions as dominating mechanism for the observed efficiency enhancement.

In summary, we report a method to boost the efficiency of BHJ OPVs by forming a compositionally graded BHJ structure with better donor/acceptor bicontinuous connection using a simple solvent-fluxing process. The formation of a graded BHJ was confirmed by multiple independent characterization methods. The PCE of the graded BHJ devices was enhanced by 15%–50% compared with the uniform distributed BHJ devices.

COMMUNICATION
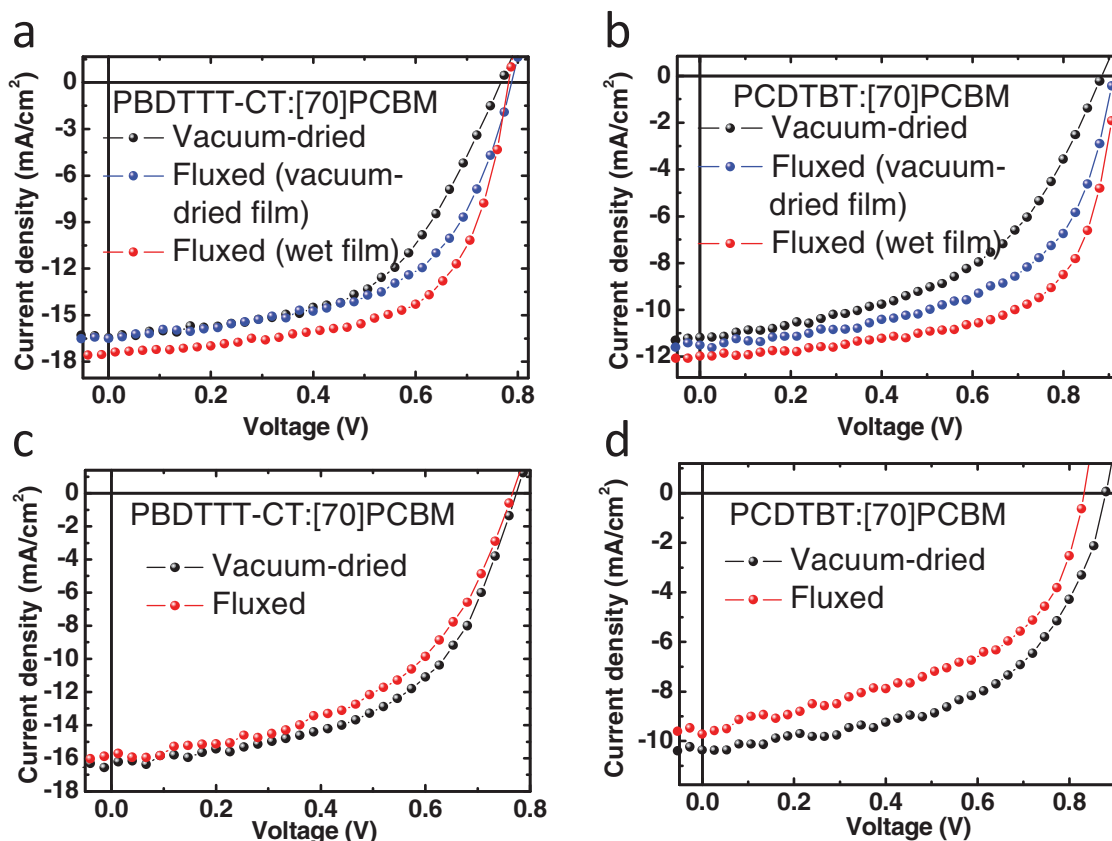
Figure 6. Photocurrent curves of the vacuum-dried (black circle line) and fluxed wet film (red circle line) and fluxed pre-vacuum-dried film (blue circle line) of PBDTTT-CT:[70]PCBM (a) and PCDTBT:[70]PCBM (b). Photocurrent curves of the vacuum-dried and solvent-fluxed inverted structure devices of PBDTTT-CT:[70]PCBM (c) and PCDTBT:[70]PCBM (d).

Experimental Section

Device Fabrication: PEDOT:PSS (Baytron-P 4083) was spin coated on clean ITO substrate at a speed of 3000 rpm. The film was then annealed at 130 °C for 30 min. Different polymer:fullerene-derivative solutions were then spin coated on top of dry PEDOT:PSS film in the N_2 filled glove box (polymers and fullerene-derivatives concentration and their spin coating parameters are described in Table S1). The blended films were fluxed by methanol or other low boiling point solvent at a spin coating speed of 2500 rpm for 20 sec. The device was finished by thermal evaporating calcium (20 nm) and aluminum (100 nm).

Blend Film Characterization: Cross-sectional TEM samples with thickness less than 100 nm were prepared with a focused ion beam at 30 kV. A current as small as 10 pA was used for final polishing in order to effectively minimize ion-beam-induced sample damage. TEM samples were examined with a Zeiss Libra 120 equipped with an in-column (Omega) energy filter. TEM experiments were performed at 120 kV, and emission current as low as 5 μA was used to minimize electron-beam-induced sample damage. Selected area electron diffraction aperture was about 1 μm in diameter, with calibration conducted using Al (111) (0.234 nm); The vertical composition profile of the blended film was quantitatively measured using a J.A Woollam Co, M-2000 variable angle spectroscopic ellipsometer. Measurements were performed between 192–1698 nm using a 300 μm diameter focused beam at angles of incidence of 55°, 65° and 75°. The optical properties of each component of the polymer blend (PBDTTT, PCDTBT, [70]PCBM) were characterized independently. The vertical composition profiles of the blended layers were then modeled using a linearly graded

effective medium approximation where the optical properties were fixed with the previously determined values. XRD measurements were performed with a Rigaku D/Max-B X-ray diffractometer with Bragg-Brentano parafocusing geometry, a diffracted beam monochromator, and a conventional copper target x-ray tube set to 40KV and 30 mA. The single path absorption was measured using an Evolution 201 UV-Visible spectrometer (thermo Scientific).

SIMS Characterization: The SIMS measurement was conducted at Evans Analytical Group. The BHJs were prepared on conductive ITO substrates or highly doped silicon substrates which were covered by PEDOT:PSS layers to avoid/reduce the charging effect. Data were calibrated in the polymer layers only. Repeat analysis on each sample was done to verify the repeat precision of the technique. The composition depth profile was extracted from the element signal when the matrix current reached a steady state, which is generally a few nms after the sputtering starts, to avoid the influence of the surface contamination or preequilibrium sputtering before the SIMS measurement.

Device Characterization: The photocurrent characteristic was measured using a calibrated Xenon-lamp-based solar simulator (Oriel 67005). EQE was measured with a Newport QE measurement kit by focusing a monochromatic beam of light onto the devices.

Supporting Information

Supporting Information is available from the Wiley Online Library or from the author.

Acknowledgements

[1] S. H. Park, A. Roy, S. Beaupré, S. Cho, N. Coates, J. S. Moon, D. Moses, M. Leclerc, K. Lee, A. J. Heeger, *Nature Photon.* **2009**, *3*, 297.

[2] F. Yang, M. Shtein, S. R. Forrest, *Nature Mater.* **2004**, *4*, 37.

[3] J. Peet, J. Kim, N. E. Coates, W. L. Ma, D. Moses, A. J. Heeger, G. C. Bazan, *Nature Mater.* **2007**, *6*, 497.

[4] Y. Zang, D. Xie, X. Wu, Y. Chen, Y. Lin, M. Li, H. Tian, X. Li, Z. Li, H. Zhu, *Appl. Phys. Lett.* **2011**, *99*, 132904.

[5] Z. He, C. Zhong, S. Su, M. Xu, H. Wu, Y. Cao, *Nature Photon.* **2012**, *6*, 593.

[6] C. E. Small, S. Chen, J. Subbiah, C. M. Amb, S. W. Tsang, T. H. Lai, J. R. Reynolds, F. So, *Nature Photon.* **2011**, *6*, 115.

[7] G. Yu, J. Gao, J. Hummelen, F. Wudl, A. Heeger, *Science* **1995**, *270*, 1789.

[8] L. Dou, J. You, J. Yang, C. C. Chen, Y. He, S. Murase, T. Moriarty, K. Emery, G. Li, Y. Yang, *Nature Photon.* **2012**, *6*, 180.

[9] L. Dou, W. H. Chang, J. Gao, C. C. Chen, J. You, Y. Yang, *Adv. Mater.* **2012**.

[10] S. Gunes, H. Neugebauer, N. S. Sariciftci, *Chem. Rev.* **2007**, *107*, 1324.

[11] B. Kannan, K. Castelino, A. Majumdar, *Nano Lett.* **2003**, *3*, 1729.

[12] A. C. Mayer, S. R. Scully, B. E. Hardin, M. W. Rowell, M. D. McGehee, *Mater. Today* **2007**, *10*, 28.

[13] X. Yang, J. Loos, S. C. Veenstra, W. J. H. Verhees, M. M. Wienk, J. M. Kroon, M. A. J. Michels, R. A. J. Janssen, *Nano Lett.* **2005**, *5*, 579.

[14] H. Hoppe, N. S. Sariciftci, *J. Mater. Chem.* **2005**, *16*, 45.

[15] Y. Liang, Z. Xu, J. Xia, S. T. Tsai, Y. Wu, G. Li, C. Ray, L. Yu, *Adv. Mater.* **2010**, *22*, E135.

[16] S. Shoaee, M. P. Eng, E. Espildora, J. L. Delgado, B. Campo, N. Martin, D. Vanderzande, J. R. Durrant, *Energy Environ. Sci.* **2010**, *3*, 971.

[17] L. G. Kaake, J. J. Jasieniak, R. C. Bakus, G. C. Welch, D. Moses, G. C. Bazan, A. J. Heeger, *J. Am. Chem. Soc.* **2012**, *134*, 19828.

[18] L. G. Kaake, D. Moses, A. J. Heeger, *J. Phys. Chem. Lett.* **2013**, *4*, 2264.

[19] B. C. Thompson, J. M. Fréchet, *Angew. Chem. Int. Ed.* **2007**, *47*, 58.

[20] M. Campoy-Quiles, T. Ferenczi, T. Agostinelli, P. G. Etchegoin, Y. Kim, T. D. Anthopoulos, P. N. Stavrinou, D. D. C. Bradley, J. Nelson, *Nature Mater.* **2008**, *7*, 158.

[21] W. Ma, C. Yang, X. Gong, K. Lee, A. J. Heeger, *Adv. Funct. Mater.* **2005**, *15*, 1617.

[22] M. Y. Chiu, U. Jeng, C. H. Su, K. S. Liang, K. H. Wei, *Adv. Mater.* **2008**, *20*.

[23] G. Li, V. Shrotriya, J. Huang, Y. Yao, T. Moriarty, K. Emery, Y. Yang, *Nature Mater.* **2005**, *4*, 864.

[24] Y. Sun, G. C. Welch, W. L. Leong, C. J. Takacs, G. C. Bazan, A. J. Heeger, *Nature Mater.* **2011**, *11*, 44.

[25] M. S. Su, C. Y. Kuo, M. C. Yuan, U. Jeng, C. J. Su, K. H. Wei, *Adv. Mater.* **2011**, *23*, 3315.

[26] D. C. Olson, Y. J. Lee, M. S. White, N. Kopidakis, S. E. Shaheen, D. S. Ginley, J. A. Voigt, J. W. P. Hsu, *J. Phys. Chem. C* **2007**, *111*, 16640.

[27] L. Koster, E. Smits, V. Mihailetchi, P. Blom, *Phys. Rev. B* **2005**, *72*, 085205.

[28] F. Monestier, J.-J. Simon, P. Torchio, L. Escoubas, F. Flory, S. Bailly, R. de Bettignies, S. Guillerez, C. Defranoux, *Sol. Energ. Mat. Sol.* **2007**, *91*, 405.

[29] A. W. Alexander Foertig, T. Gerbich, D. Cheyns, a. C. D. Vladimir Dyakonov, *Adv. Energ. Mater.* **2012**, *2*, 1483.

[30] C. J. Brabec, N. S. Sariciftci, J. C. Hummelen, *Adv. Funct. Mater.* **2001**, *11*, 15.

[31] A. Baumann, T. J. Savenije, D. H. K. Murthy, M. Heeney, V. Dyakonov, C. Deibel, *Adv. Funct. Mater.* **2011**, *21*, 1687.

[32] R. A. Street, A. Krakaris, S. R. Cowan, *Adv. Funct. Mater.* **2012**, *22*, 4608.

[33] J. K. J. van Duren, X. Yang, J. Loos, C. W. T. Bulle Lieuwma, A. B. Sieval, J. C. Hummelen, R. A. J. Janssen, *Adv. Funct. Mater.* **2004**, *14*, 425.

[34] S. R. Cowan, N. Banerji, W. L. Leong, A. J. Heeger, *Adv. Funct. Mater.* **2012**, *22*, 1116.

[35] Z. Xu, L. M. Chen, G. Yang, C. H. Huang, J. Hou, Y. Wu, G. Li, C. S. Hsu, Y. Yang, *Adv. Funct. Mater.* **2009**, *19*, 1227.

[36] H. Lu, B. Akgun, T. P. Russell, *Adv. Energ. Mater.* **2011**, *1*, 870.

[37] T.-H. K. Ming-Kun Lee, K.-W. Kong, Y.-R. Hong, J.-C. Wang, H.-F. M. Sheng-Fu Horng, *Synt. Met.* **2012**, *162*, 1930.

[38] C. Deibel, A. Wagenpfahl, V. Dyakonov, *Phys. Rev. B* **2009**, *80*, 075203.

[39] S. R. Cowan, A. Roy, A. J. Heeger, *Phys. Rev. B* **2010**, *82*, 245207.

[40] S. J. Lou, J. M. Szarko, T. Xu, L. Yu, T. J. Marks, L. X. Chen, *J. Am. Chem. Soc.* **2011**, *133*, 20661.

[41] Y. Yao, J. Hou, Z. Xu, G. Li, Y. Yang, *Adv. Funct. Mater.* **2008**, *18*, 1783.

[42] L. F. Drummy, R. J. Davis, D. L. Moore, M. Durstock, R. A. Vaia, J. W. Hsu, *Chem. Mat.* **2010**, *23*, 907.

[43] J. Chen, X. Yu, K. Hong, J. M. Messman, D.L. Picklel, K. Xiao, M. D. Dadmun, J. W. Mays, A. J. Rondinone, B. G. Sumpter, S. M. Kilbey *J. Mater. Chem.* **2012**, *22*, 13013.

[44] J. Ajuria, S. Chavhan, R. Tena-Zaera, J. Chen, A.J. Rondinone, P. Sonar, A. Dodabalapur, R. Pacios, *Organic Electronics* **2013**, *14*, 326.

[45] D. Aspnes, *Thin Solid Films* **1982**, *89*, 249.

[46] H. Zhou, Y. Zhang, J. Seifter, S. D. Collins, C. Luo, G. C. Bazan, T. Q. Nguyen, A. J. Heeger, *Adv. Mater.* **2013**, *25*, 1646.